Electronic Supplementary Material (ESI) for Inorganic Chemistry Frontiers.
This journal is © the Partner Organisations 2020

# *Supporting Information (SI)*

## Preparation of $Bi_2MoO_6/Ti_3C_2$ MXene Heterojunction Photocatalyst for Fast Tetracycline Degradation and Cr(VI) Reduction

Danxia Zhao[a] and Chun Cai * [a]

[a] *Chemical Engineering College, Nanjing University of Science & Technology, 200 Xiaolingwei, Nanjing 210094, P. R. China**

Tel.: +86-25-84315514; Fax: +86-25-84315030 ; e-mail: c.cai@njust.edu.cn

.

**Section S1:** Experimental, Characterization, Photocatalytic measurement Methods.

**Fig.S1** Schematic of the $Ti_3C_2$ nanosheet and $Bi_2MoO_6/Ti_3C_2$ composite synthesis.

**Fig. S2** $N_2$ adsorption–desorption isotherms and Barrett–Joyner–Halenda (BJH) pore size distribution (inserted one) of $Bi_2MoO_6$ and the $Bi_2MoO_6/Ti_3C_2$ samples.

**Fig. S3** (a), UV–vis diffuse reflectance spectra of $Bi_2MoO_6$, and $Bi_2MoO_6/Ti_3C_2$ composites with different compositions, (b) plots of $(\alpha h\nu)^2$ vs $(h\nu)$ for $Bi_2MoO_6$.

**Figure S4.** (a) XPS-VB spectra of $Bi_2MoO_6$; (b) Mott-Schottky plot of $Bi_2MoO_6$.

**Figure S5.** The pseudo-first-order kinetics fitting curves and apparent rate constants over different catalysts (a) TC; (b) Cr(VI).

**Fig. S6** Proposed intermediates and degradation routes of TC with light-induced $h^+$,•OH and $\bullet O_2^-$.

**Figure S7.** The UV–vis absorption spectral changes of Cr(VI) solution over the BT-30 sample at pH of (a) 6.0, and (b)10.0. Reaction conditions: Cr(VI) concentration = 15 mg/L, catalyst dosage=0.5 g/L, 15W white LED lamp.

**Figure S8.** Stability test of photodegradation of TC and Cr(VI) over BT-30 (a).

**Figure S9.** XRD (a), TEM images (b) before and after the photocatalytic reaction.

**Figure S10.** Charge distribution of the adsorption models.

**Figure S11.** Transient photocurrent measurements of $Bi_2MoO_6$, $Bi_2MoO_6/Ti_3C_2$ composite (BT-30) and LBT-30.

**Table S1.** Specific surface area, pore size and pore volume of as-prepared samples.

**Table S2.** Binding energies of Ti 2p in $Ti_3C_2$ and BT-30.

**Section S1.**

## Experimental Methods

### Preparation of $Ti_3C_2$ MXene

Typically, 2 g $Ti_3AlC_2$ powders were slowly added into 40 mL40 wt % HF solution and then stirred at room temperature for 72 h. The precipitate was centrifuged and washed by D.I. water several times, and then the obtained $Ti_3C_2$ MXene powder was dried under vacuum at 60 °C. The obtained dried sample was re-dispersed in 20 mL of DMSO with stirring at room temperature overnight. The suspension was then centrifuged and washed four times with D.I.water. The collected solid was dispersed in deionized water at a mass ratio of 1: 100 and sonicated for 5 hours. The suspension was then centrifuged at 3500 rpm for 5 h to remove unexfoliated residue. Finally, the supernatant of $Ti_3C_2$ nanosheets was obtained. The concentration of the resulting supernatant was measured as 1 mg $mL^{-1}$. The obtained $Ti_3C_2$ MXene powder has not been sonicated labeled as layer $Ti_3C_2$.

### Preparation of $Bi_2MoO_6$ /$Ti_3C_2$

To prepare of $Bi_2MoO_6$/$Ti_3C_2$ composites, a certain amount of Ultrathin $Ti_3C_2$ nanosheets, 0.3 g CTAB and 0.970 g of $Bi(NO_3)_3 \cdot 5H_2O$ were dispersed into 70 mL D.I. water and sonicated for 30 min. After that, 0.242 g of $Na_2MoO_4 \cdot 2H_2O$ was added to the reacted system. After magnetically stirring for 6 h and adjusting pH to 7, the mixture was transferred to Teflon-lined autoclave and heated to 180 °C for 16 h. The grayish yellow precipitations were obtained. The different weight ratio of $Bi_2MoO_6$ and $Ti_3C_2$ was set as 500:10, 500:30 and 500:50, which marked as BT-10, BT-30 and BT-50 respectively. For comparison, the weight ratio of $Bi_2MoO_6$ and Layer $Ti_3C_2$ was set as 500:30, which labeled as LBT-30. 2D $Bi_2MoO_6$ were prepared under the same conditions without $Ti_3C_2$.

### Characterization of photocatalysts

X-ray diffractometry (XRD) using a Shimadzu XRD-6000 diffractometer with Cu Kα irradiation. Scanning electron microscopy (SEM) images was performed using a Hitachi S-4800. TEM images were taken using a PHILIPS Tecnai 12 microscope operating at 120 kv. Energy Dispersive X-ray Spectroscopic analysis (EDS) was performed with a JEM-2010(HR) transmission electron microscope at an acceleration voltage of 200kV. High Resolution Transmission electron microscopy (HRTEM) was performed on Philips-FEI Tecnai G2 F20 operating at 300kv. Nitrogen adsorption-desorption analysis was conducted using a Micromeritics ASAP 2020 at 77 K. The specific surface areas were calculated by the Brunauer-Emmett-Teller (BET) method. In addition, X-ray photoelectron spectroscopy (XPS) was performed on an ESCALAB 250Xi spectrometer, using an Al Kα X-ray source (1486.6 eV of photons), which was calibrated by setting the C 1s peak to 284.80 eV. The UV - Vis diffuse reflectance spectra of the catalysts were recorded on a UV - Vis spectrometer (Lambda 750) within the range of 200 - 1100 nm. Photoluminescence spectra (PL) of the catalysts were carried out on a spectrophotometer (LabRAM HR

Evolution).

**Electrochemical measurements**

Electrochemical and photoelectrochemical measurements were carried out on an electrochemical workstation (CHI 660E, Shanghai) with a standard three-electrode system. The powder coated on indium-tin-oxide (ITO) glass substrate was applied as the working electrode. 10 mg powder was suspended into 1 mL absolute ethanol and then the slurry was dropwise added on a ITO substrate (15mm × 30 mm). The working electrode was exposed to air for 10 h to remove the ethanol. Platinum wire and Ag/AgCl electrode were used as the counter electrode and reference electrode, respectively. The electrolyte was 0.1 M $Na_2SO_4$ solution and illumination source was a 300 W Xe lamp providing simulated solar light.

**ESR experiment**

The ·OH and $\cdot O_2^-$ radical signals in solution during the photocatalytic process under visible light ($\lambda >$ 420 nm) were determined using electron spin resonance (ESR; JES FA200).

**Computational Details**

The functional of gradient approximation (GGA) and Perdew, Burke, and Ernzerhof (PBE) was used throughout to describe the electron–electron exchange and correlation interactions. For the k-point sampling of Brillouin zone integrals, a (2 × 1× 2) k-point grid was used, and meanwhile, cutoff energy 500 eV was used as the maximum value from all the cutoffs specific to each element in this system. The convergence tolerance of an energy of $10^{-5}$ eV was taken, and the relaxation of the unit cell, including the atoms, was performed by Geometry Optimization. And the formula to calculate the adsorption energy is that

$$E_{ad} = E_{tot} - E_a - E_s$$

Where Ead is the adsorption energy, and $E_{tot}$ is the total energy of adsorbed molecules and UIO. $E_a$ and $E_s$ is the the energy of adsorbed molecules and $Ti_3C_2/Bi_2MoO_6$, respectively.

**Photocatalytic experiments**

Photocatalytic degradation of Cr (VI, 15 mg/L) and Tetracycline (TC, 15 mg/L) were performed as follows. In each experiment, 10 mg of catalyst were added to the above pollutant solutions (20 mL). Before the reaction, the suspension was magnetically stirred for 40 min in the dark to attain adsorption–desorption equilibrium. During the white LED lamp (50W, $\lambda >$ 400 nm) irradiation, aliquots (2 mL) were obtained at specific times from the reaction suspension and centrifuged to remove the photocatalysts. The concentration of TC-HCl was measured at 356 nm and the content of Cr(VI) was determined by the diphenylcarbazide colorimetry method at 540 nm using a UV-vis spectrophotometer. In addition, the pH of Cr(VI) initial solution was adjusted by $1MH_2SO_4$ or 1M NaOH solution.

The intermediates produced in the photodegradation process of TC were identified by high performance liquid chromatography-mass spectrometry (LC/MS). Mobile phase was a mixture of

acetonitrile and formic acid (0.1%) with a flow rate of 0.25mL/min. The injection volume was 5.0 μL. The fragment voltage was 135 V and the capillary voltage was 2800 V. The mass range of the MS is m /z 100-600.

Free radical trapping experiments were based on the above experimental operations. Ethylenediaminetetraacetic acid disodium salt (EDTA-2Na), potassium persulfate ($K_2S_2O_8$), tert-butyl alcohol (TBA) and benzoquinone (BQ) as scavengers for photogenerated holes, photogenerated electrons, hydroxyl radicals and superoxide radicals, respectively.

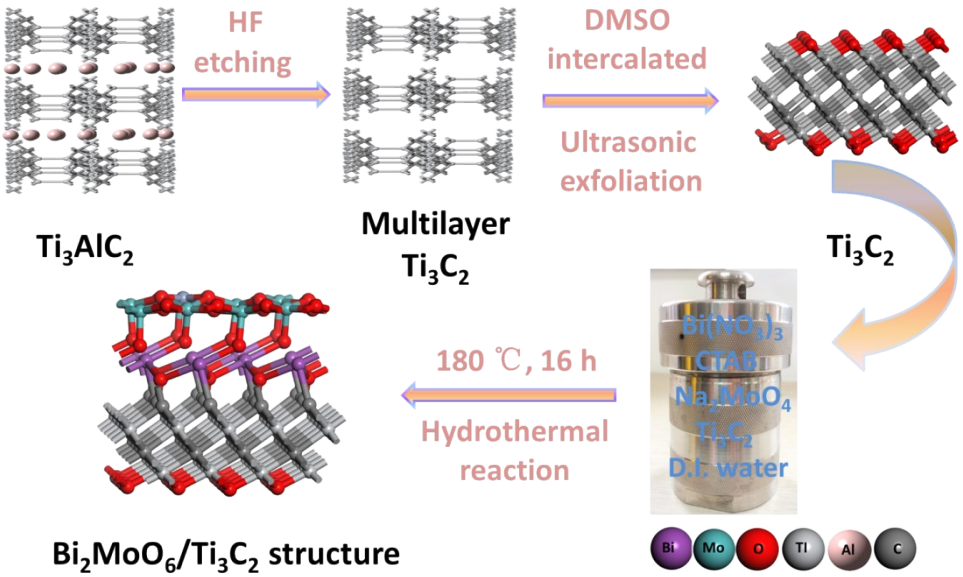


**Fig.S1** Schematic of the $Ti_3C_2$ nanosheet and $Bi_2MoO_6/Ti_3C_2$ composite synthesis.

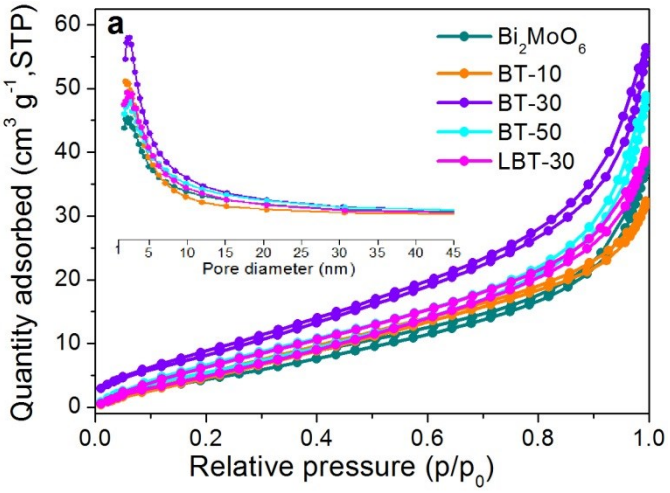


**Fig. S2** $N_2$ adsorption–desorption isotherms and Barrett–Joyner–Halenda (BJH) pore size distribution (inserted one) of $Bi_2MoO_6$ and the $Bi_2MoO_6/Ti_3C_2$ samples.

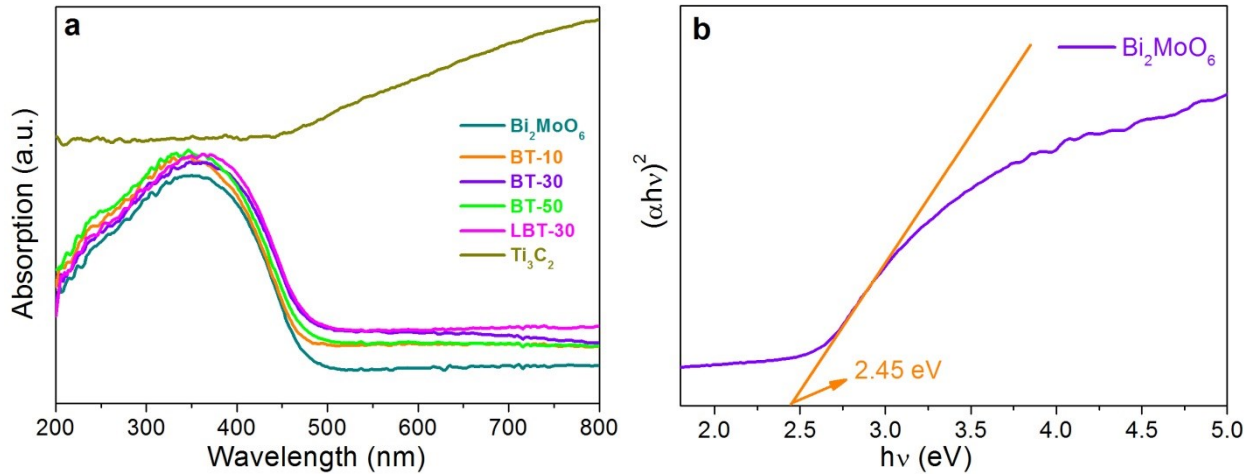


**Fig. S3** (a), UV–vis diffuse reflectance spectra of $Bi_2MoO_6$, and $Bi_2MoO_6/Ti_3C_2$ composites with different compositions, (b) plots of $(\alpha h\nu)^2$ vs $(h\nu)$ for $Bi_2MoO_6$.

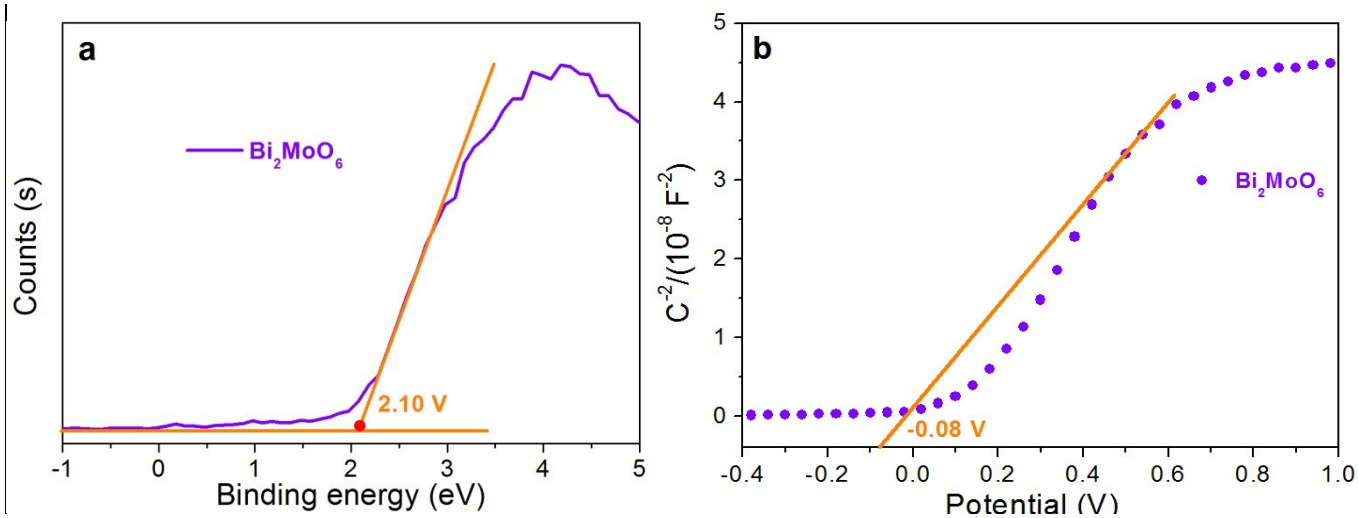


**Fig. S4.** (a) XPS-VB spectra of $Bi_2MoO_6$; (b) Mott-Schottky plot of $Bi_2MoO_6$.

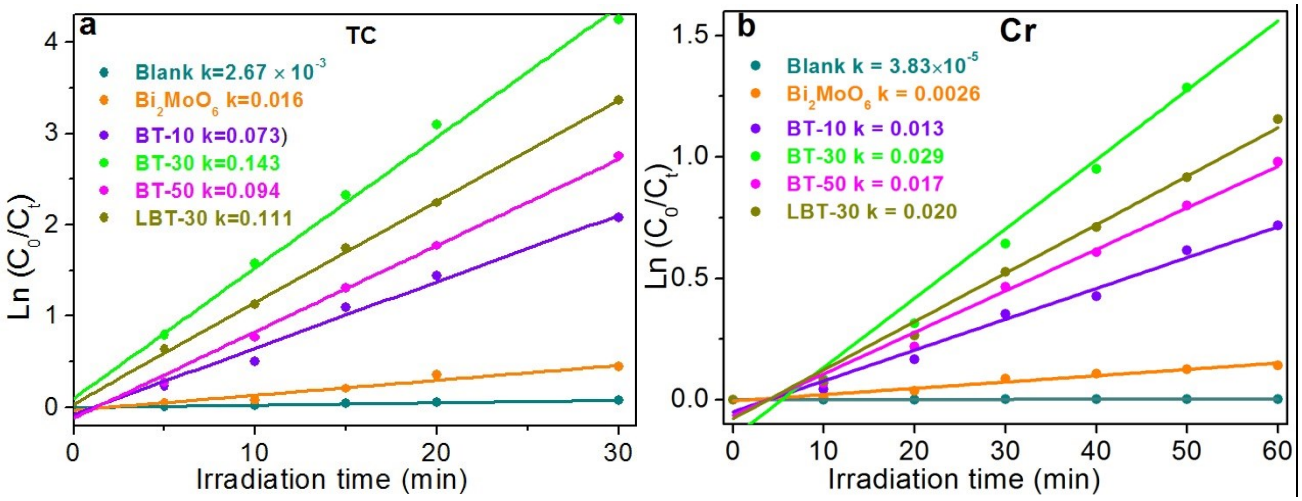


**Fig. S5.** The pseudo-first-order kinetics fitting curves and apparent rate constants over different catalysts (a) TC; (b) Cr(VI).

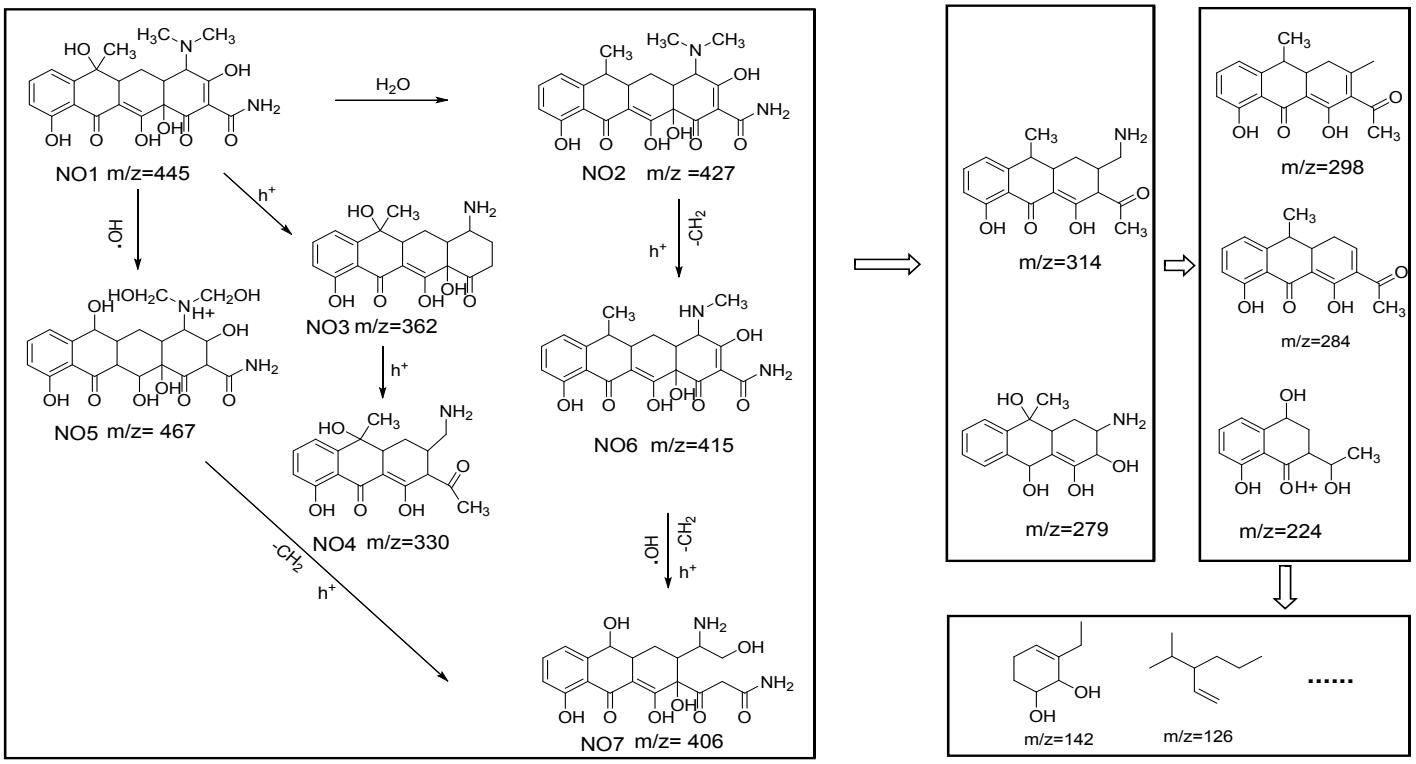


**Fig. S6** Proposed intermediates and degradation routes of TC with light-induced $h^+$,•OH and $•O_2^-$.

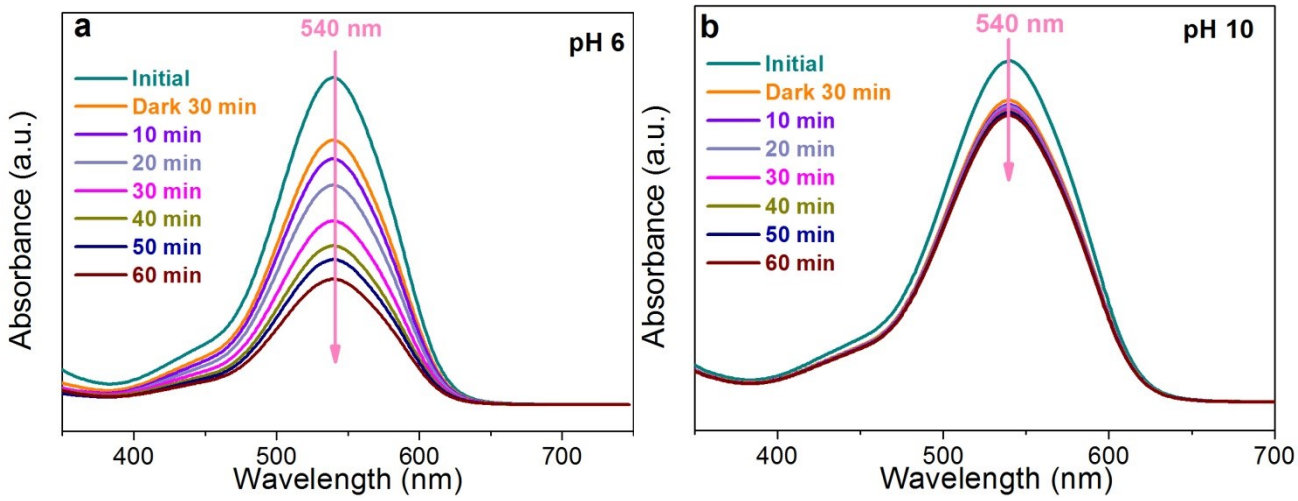


**Fig. S7.**The UV–vis absorption spectral changes of Cr(VI) solution over the BT-30 sample at pH of (a) 6.0, and (b)10.0. Reaction conditions: Cr(VI) concentration = 15 mg/L, catalyst dosage=0.5 g/L, 150W white LED lamp.

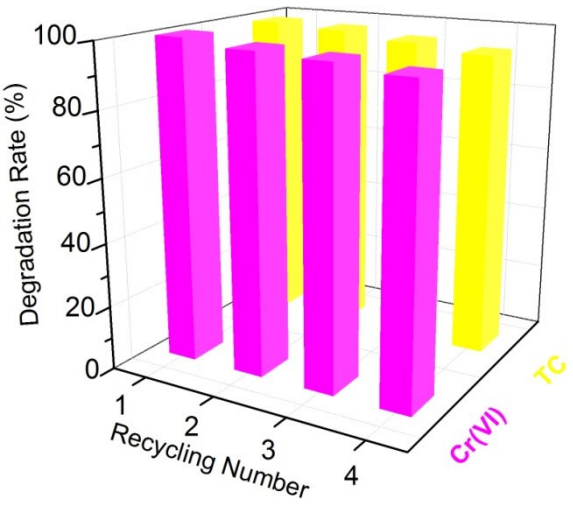


**Fig. S8** Stability test of photodegradation of TC and Cr(VI) over BT-30 (a).

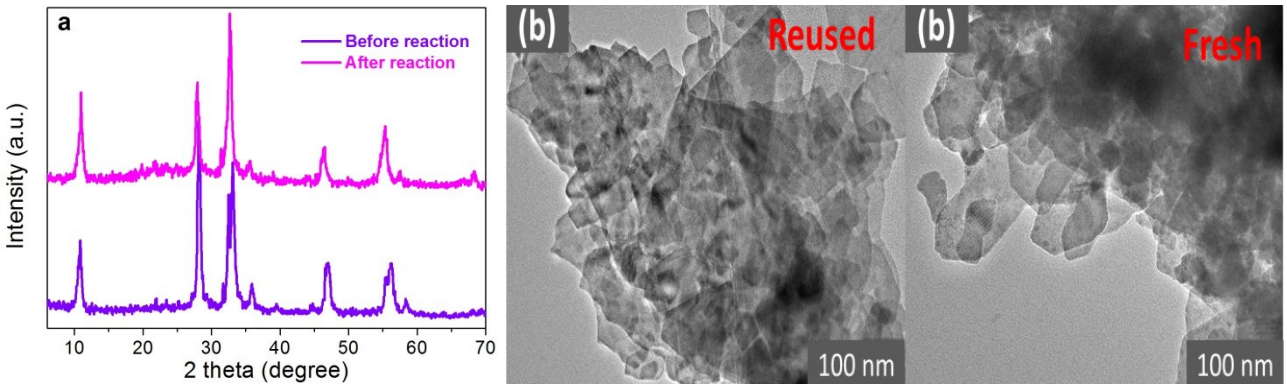


**Fig. S9.** XRD (a), TEM images (b) before and after the photocatalytic reaction.

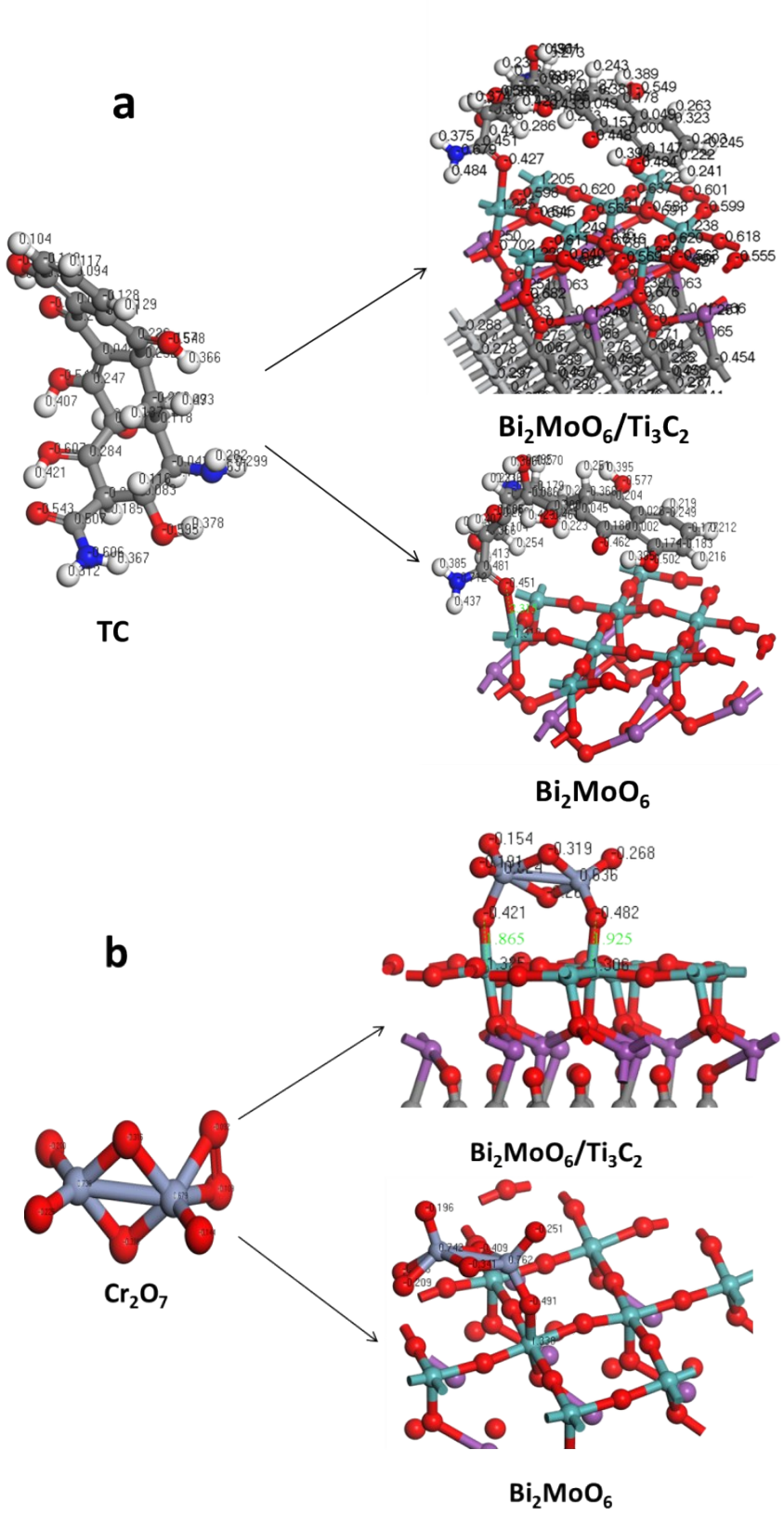


**Fig. S10.** Charge distribution of the adsorption models.

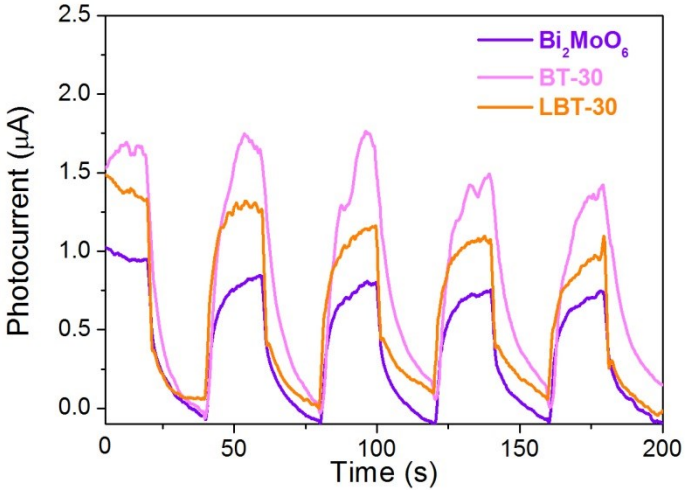


**Fig. S11.** Transient photocurrent measurements of $Bi_2MoO_6$, $Bi_2MoO_6/Ti_3C_2$ composite (BT-30) and LBT-30.

**Table S1**. Specific surface area, pore size and pore volume of as-prepared samples.

| samples | $S_{BET}$ ($m^2$ $g^{-1}$) | Pore size (nm) | Total pore volume ($cm^3$ $g^{-1}$) |
|---|---|---|---|
| $Bi_2MoO_6$ | 20.70 | 0.055 | 10.70 |
| BT-10 | 26.84 | 0.047 | 7.069 |
| BT-30 | 33.24 | 0.084 | 9.79 |
| BT-50 | 25.40 | 0.071 | 11.11 |
| MBT-10 | 25.93 | 0.057 | 9.10 |

**Table S2**. Binding energies of Ti 2p in $Ti_3C_2$ and BT-30.

| BE (eV) of $Ti_3C_2$ | BE (eV) of UBT-30 | Assigned to | Reference |
|---|---|---|---|
| 454.8 | | Ti (3) $2P_{3/2}$ | [1, 2] |
| 455.6 | 455.2 | Ti (2) $2P_{3/2}$ Ti-C | [1] |
| 456.6 | 456.4 | Ti (2) $2P_{3/2}$ | [2] |
| 459.2 | 459.0 | Ti (4) $2P_{3/2}$ $TiO_2$ | [3] |
| 461.1 | 461.0 | Ti (2) $2P_{1/2}$ Ti-C | [4] |
| 462.3 | | Ti (3) $2P_{1/2}$ | [5] |
| 464.9 | 464.3 | Ti (4) $2P_{1/2}$ $TiO_2$ | [6] |

## References


1. V. Schier, H. J. Michel and J. Halbritter, ARXPS-analysis of sputtered TiC, SiC and $Ti_{0.5}Si_{0.5}C$ layers, *Fresenius' J. Anal. Chem.*, 1993, **346**, 227-232.
2. F. Santerre, M. A. El Khakani, M. Chaker and J. P. Dodelet, Properties of TiC thin films grown by pulsed laser deposition, *Appl. Surf. Sci.*, 1999, **148**, 24-33.
3. T. Sultana, G. L. Georgiev, G. Auner, G. Newaz, H. J. Herfurth and R. Patwa, XPS analysis of laser transmission micro-joint between poly (vinylidene fluoride) and titanium, *Appl. Surf. Sci.*, 2008, **255**, 2569-2573.
4. S. Cao, B. Shen, T. Tong, J. Fu and J. Yu, 2D/2D Heterojunction of Ultrathin MXene/$Bi_2WO_6$ Nanosheets for Improved Photocatalytic $CO_2$ Reduction, *Adv. Funct. Mater.*, 2018, **28**, 1800136.
5. J. Low, L. Zhang, T. Tong, B. Shen and J. Yu, $TiO_2$/MXene $Ti_3C_2$ composite with excellent photocatalytic $CO_2$ reduction activity, *J. Catal.*, 2018, **361**, 255-266.
6. T. Cai, L. Wang, Y. Liu, S. Zhang, W. Dong, H. Chen, X. Yi, J. Yuan, X. Xia, C. Liu and S. Luo, $Ag_3PO_4$/$Ti_3C_2$ MXene interface materials as a Schottky catalyst with enhanced photocatalytic activities and anti-photocorrosion performance, *Appl. Catal., B*, 2018, **239**, 545-554.